



HAL
open science

CFD simulations in mechanically stirred tank and flow field analysis application to the wastewater (sugarcane vinasse) anaerobic digestion

Hélène Caillet, Laetitia Adelard, Alain Bastide

► **To cite this version:**

Hélène Caillet, Laetitia Adelard, Alain Bastide. CFD simulations in mechanically stirred tank and flow field analysis application to the wastewater (sugarcane vinasse) anaerobic digestion. Wastewater Treatment, In press. hal-02982117

HAL Id: hal-02982117

<https://hal.science/hal-02982117>

Submitted on 28 Oct 2020

HAL is a multi-disciplinary open access archive for the deposit and dissemination of scientific research documents, whether they are published or not. The documents may come from teaching and research institutions in France or abroad, or from public or private research centers.

L'archive ouverte pluridisciplinaire **HAL**, est destinée au dépôt et à la diffusion de documents scientifiques de niveau recherche, publiés ou non, émanant des établissements d'enseignement et de recherche français ou étrangers, des laboratoires publics ou privés.

We are IntechOpen, the world's leading publisher of Open Access books Built by scientists, for scientists

5,000

Open access books available

125,000

International authors and editors

140M

Downloads

Our authors are among the

154

Countries delivered to

TOP 1%

most cited scientists

12.2%

Contributors from top 500 universities



WEB OF SCIENCE™

Selection of our books indexed in the Book Citation Index
in Web of Science™ Core Collection (BKCI)

Interested in publishing with us?
Contact book.department@intechopen.com

Numbers displayed above are based on latest data collected.
For more information visit www.intechopen.com



Chapter

CFD Simulations in Mechanically Stirred Tank and Flow Field Analysis: Application to the Wastewater (Sugarcane Vinasse) Anaerobic Digestion

Hélène Caillet, Alain Bastide and Laetitia Adelard

Abstract

Anaerobic digestion is a widely used process for waste treatment and energy production. This natural process takes place in a controlled environment, anaerobic digesters. Mixing is one of the main operating parameters. The understanding of the flows during the agitation of the medium is crucial for the optimization of the process yield. In fact, the mass and heat transfers are enhanced by the agitation. However, the complex biochemical reactions can be inhibited with overly vigorous agitation. A detailed and in-depth understanding of the phenomena occurring during agitation requires modeling studies. In this chapter, we propose a general approach, based on computational fluid mechanics (CFD), to analyze the mechanical mixing of an anaerobic reactor. We apply this work to the anaerobic digestion of the sugarcane vinasse, which is a liquid waste generated during the production of alcohol. The single-phase Reynolds-averaged Navier-Stokes (RANS) simulations of mechanical agitation of Newtonian fluids for different rotational speeds are presented. The equations system is closed with the standard k-epsilon turbulence model. The flow field is analyzed with the velocity profiles, the Q and Lambda2 fields, the pressure and the vorticity.

Keywords: anaerobic digestion, computational fluid dynamics (CFD), Newtonian, mechanical mixing, vinasse, RANS

1. Introduction

Anaerobic digestion is a widely used process for organic waste treatment, such as manure, sludge or biowaste. This natural process is based on the digestion of the material in five biological reactions. Each reaction involves a specific group of micro-organisms. First, the complex polymers are hydrolyzed into water-soluble monomers and oligomers by the hydrolytic and fermentative bacteria. Then, the acidogenesis consists in the transformation of the soluble organic molecules into volatile fatty acids, organic acids, hydrogen, carbon dioxide, alcohols and acetate by acidogenic bacteria [1, 2]. This reaction is followed by the acetogenesis, during which the products of hydrolysis and acidogenesis are converted into acetate and

carbon dioxide by the action of acetogenic bacteria [1, 2]. Finally, the methanogenesis, the last step of the degradation process, forms methane through two metabolisms. Acetotrophic methanogens transform acetate into methane and carbon dioxide, while hydrogen methanogens combine hydrogen and carbon dioxide to form methane and water [1, 2]. On a laboratory or industrial scale, this natural process takes place in a controlled environment in anaerobic digesters. The main operating parameters are temperature, agitation, organic load and hydraulic retention time.

Anaerobic digestion is based on a set of biological reactions under the action of various groups of micro-organisms. Therefore, the contact between the organic matter and each group of microorganisms must be guaranteed to provide biogas production. This condition is met in the case of adequate digester agitation. The stirring system is used in order to enhance mass and heat transfers. The stirring can be done by recirculation of gas or leachate or mechanical system. The understanding of the flows during the agitation of the medium is crucial for (1) the comprehension of the impact on biochemical reactions and (2) the optimization of the mixing system. According to the choice of agitation mode, the medium can be well-agitated, homogenous or there might be presence of dead zones or isolated turbulent zones. In this context, the flow analysis by numeric approach is a promising method to identify these zones and two main issues occur. First, to promote the anaerobic digestion process, it is necessary to limit the volume of dead zones without stirring too vigorously. In fact, in the dead zones, the organic matter could be not digested due to the lack of contact between the substrate and each group of micro-organisms. In this sense studies are being conducted to evaluate the volume and the position of dead zones with the aim of reducing their volumes [3–5]. Second, in the case of highly mixed zones could imply the destruction of the methanogenic centers and inhibit the biochemical reactions. As a consequence, it is evident that anaerobic digestion yields can be improved by the agitation optimization.

The qualitative description of the effect of flow velocity on the biogas yield is illustrated in **Figure 1**.

As a matter of fact, the properties of the medium are impacted by the mixture type. Consequently, the fluid characterization is an important factor. In this work, we propose first to study the mechanical parameter of the sugarcane vinasse, with the consideration of the rheology of the digestion medium. The sugarcane vinasse is a liquid waste generated from the alcohol production. In the case of liquid digestion, defined by a solids content of less than 15%, the medium may both have a Newtonian or non-Newtonian behavior. The behavior of the fluid has a direct consequence on the flows within the digester. Depending on the waste type, the digestion medium will also have a different viscosity. Viscosity is the term to express the resistance of a fluid to flow and motion. It is assumed that the sugarcane vinasse is Newtonian [6].

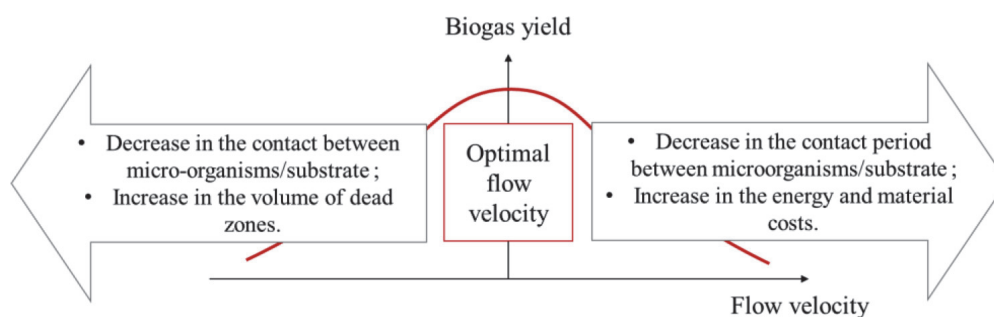


Figure 1.
Qualitative description of the effect of flow velocity on the biogas yield.

In order to model the flows within a digester, it is therefore necessary to know both its technical characteristics (geometry, stirring mode) and the fluid properties. All these choices will have an incidence on the mechanical energy and thus on the expended electrical energy to produce methane.

Consequently, the CFD simulations allow to analyze the flows within a digester of a specific waste mixture, considering its rheological properties. In the literature, the CFD models developed are based on the Reynolds-averaged Navier-Stokes (RANS) equations, the large eddy simulation (LES) as well as direct numerical simulation (DNS). DNS method provides the more precise results by solving directly the Navier-Stokes equations but it is also the most time-consuming method. RANS and LES are specific methods developed for turbulence studies. They are both used by many authors. LES method is more time-consuming than RANS method but provides more accurate outcomes. For example, Fan and al. used RANS method for simulating the hydrodynamic behaviors in a stirred tank [7], and Foukrach et al. used RANS method for studying mixing performance in a gas-mixed anaerobic digester [8].

In the current work, we propose a case study on the vinasse. The RANS approach is used, closed with the standard k-epsilon turbulence model. Simulations for different rotational speeds are carried out in order to analyze the flow field in mechanically stirred digester in function of the rotational speed.

2. Theoretical model

2.1 Assumptions

The anaerobic digestion occurs at the mesophilic regime at 37°C. As previously said, it is assumed that the sugarcane vinasse is Newtonian [6] and the fluid is isothermal and incompressible. The rheological properties of the medium are related to the total solid (TS) content of the substrates. The properties of the substrate are detailed in the following part in the **Table 1**.

In the present study, we consider single-phase turbulent flow.

The sugarcane vinasse from the Rivière du Mât distillery is a recalcitrant waste with a chemical oxygen demand (COD) of 86.70 g_{O₂}.L⁻¹, 6.64% TS content, 4.04% volatile solid content and a pH of 4.84 [10]. The biochemical methane potential is 185.59 NL_{CH₄}.kg_{COD}⁻¹ [10].

In the next section, we present the geometry used in this work and the mesh generation suitable to the mechanical agitation study.

2.2 Geometry and mesh

This study is carried out on an existing geometry in literature. Based on the study carried out by Wu [11], the geometry consists in a 260 mm height tank (liquid

Fluid	Density (kg.m ⁻³)	Dynamic viscosity (Pa.s)	Sources
Vinasse	1044.69	0.0010097	[6]
Water	1000	0.001	
Screened and diluted dairy cow manure	1000	0.0009	[9]

Table 1.
Rheological properties of Newtonian fluids.

zone. These two boundaries are identical and have the same initial and boundary conditions. The rotational speed is assigned directly to the moving zone.

The mathematical model is based on RANS equations associated with the forces linked to the impeller rotation: the Coriolis and centrifugal forces. The governing equations for the rotating zone and the stationary zone are respectively:

$$\begin{cases} \frac{\partial u_R}{\partial t} + \nabla \cdot (u_R \otimes u_I) = -\nabla p + \nabla \cdot \left(\nu_{eff} \left(\nabla u_I + (\nabla u_I)^T \right) \right) \\ \nabla \cdot u_R = 0 \end{cases} \quad (1)$$

$$\begin{cases} \frac{\partial u_I}{\partial t} + \nabla \cdot (u_I \otimes u_I) = -\nabla p + \nabla \cdot \left(\nu_{eff} \left(\nabla u_I + (\nabla u_I)^T \right) \right) \\ \nabla \cdot u_I = 0 \end{cases} \quad (2)$$

where u_I and u_R are the absolute velocities viewed respectively from the stationary and the rotating frames (m.s^{-1}), t is the time (s), ν_{eff} is the effective kinematic viscosity ($\text{m}^2.\text{s}^{-1}$) and p is the pressure (Pa).

The incompressible solvers on OpenFoam use the modified pressure (kinematic pressure) P ($\text{m}^2.\text{s}^{-2}$), calculated by the following equation:

$$P = \frac{p}{\rho} \quad (3)$$

where p is the pressure ($\text{kg.m}^{-1}.\text{s}^{-2}$) in and ρ the fluid density (kg.m^{-3}).

The system is closed with the standard $k - \varepsilon$ turbulence model, where k is the turbulent kinetic energy ($\text{m}^2.\text{s}^{-2}$) and ε is the turbulent dissipation ($\text{m}^2.\text{s}^{-3}$). The model implemented in OpenFOAM does not include the buoyancy contribution. The two equations of this model are:

$$\frac{\partial}{\partial t}(k) = \nabla \cdot (D_k \nabla k) + G_k - \frac{2}{3}(\nabla \cdot u)k - \varepsilon + S_k \quad (4)$$

$$\frac{\partial}{\partial t}(\varepsilon) = \nabla \cdot (D_\varepsilon \nabla \varepsilon) + \frac{C_1 G_k \varepsilon}{k} - \left(\frac{2}{3} C_1 - C_{3,RDT} \right) (\nabla \cdot u) \varepsilon - C_2 \frac{\varepsilon^2}{k} + S_\varepsilon \quad (5)$$

where u is equal to u_I or u_R , S_k is the internal source term for k , S_ε is the internal source term for ε , G_k is the production of k , C_1 and C_2 are model constants, D_k the effective diffusivity for k and D_ε is the effective diffusivity for ε . The values of the model constants used in OpenFoam, as in the standard model are: $C_\mu = 0.09$, $C_1 = 1.44$, $C_2 = 1.92$, $\sigma_k = 1$ and $\sigma_\varepsilon = 1.3$ [15].

The production term G_k is:

$$G_k = \nu_t S^2 \quad (6)$$

The assumption of the standard $k - \varepsilon$ turbulence model turbulence is the following expression of the turbulent viscosity ν_t ($\text{m}^2.\text{s}^{-1}$):

$$\nu_t = C_\mu \frac{k^2}{\varepsilon} \quad (7)$$

For the initialization of the numerical simulations, the turbulent kinetic energy for isotropic turbulence k_0 and the turbulent dissipation rate ε_0 are calculated as follows:

$$k_0 = \frac{3}{2} (I |u_{ref}|)^2 \quad (8)$$

$$\varepsilon_0 = \frac{C_\mu^{0.75} k_0^{1.5}}{L} \quad (9)$$

where I (%) is the turbulence intensity with a default value of 0.05, u_{ref} (m.s⁻¹) is a reference velocity (the stirring velocity) and L (m) is the reference length scale (the digester radius).

The mesh must be refined at the walls. In fact, the standard turbulent model is derived under the assumption of a high local turbulent Reynolds number [16]. This low turbulent Reynolds number region is called the viscous sub layer. Launder and Spalding suggested the following wall function equation [15] to reduce cell number in these zones:

$$u^+ = \frac{1}{\kappa} \ln y^+ + C \quad (10)$$

where $u^+ = |u|/u_T$ is the dimensionless velocity where u_T is the friction velocity (or shear velocity). $y^+ = u_T y/\nu$ is the dimensionless local Reynolds number where y is the width of the boundary layer (normal distance from the wall). The range of the local Reynolds number is $11.06 \leq y^+ \leq 300$ [17]. Platteeuw et al. recommend that the local Reynolds number of the first cell should be in the range of $20 \leq y^+ \leq 100$ [16]. κ is the von Karman constant and C is a parameter related to the wall roughness. In the case of smooth walls, the values are respectively 0.419 and 5.24.

The boundary conditions are:

$$\begin{aligned} \text{No slip: } u = 0, \quad \frac{\partial p}{\partial n} = 0, \quad \text{on } \Gamma_0 \\ \text{Imposed velocity field: } v_r = \omega R, \quad \frac{\partial p}{\partial n} = 0, \quad \text{on } \Gamma_1 \end{aligned} \quad (11)$$

where the index r is the center of the elementary surfaces of each cell the agitator, ω is the angular velocity, R is the impeller radius, Γ_0 is the digester walls and Γ_1 is the impeller walls.

The rotational speed of the agitator is defined by the speed of rotation of the mobile zone of the mesh. A sudden increase in the stirring speed at the first time step causes a sharp increase in the CFL. Thus, a velocity ramp is necessary for the simulations starting to maintain the Courant number lower than 0.5.

2.4 Rheological expression

We refer to the pseudo-plastic model of Ostwald. It allows to express the shear stress τ (Pa) as a function of the shear rate $\dot{\gamma}$ (s⁻¹). It is calibrated by two parameters: the consistency index k (Pa.s ^{n}) and the flow index n . It is expressed as follows:

$$\tau = k \dot{\gamma}^n \quad (12)$$

The viscosity is expressed as follows:

$$\eta = k \dot{\gamma}^{n-1} \quad (13)$$

The components of the tensor of the shear rate are:

$$\dot{\gamma}_{ij} = \left(\frac{\partial u_i}{\partial x_j} + \frac{\partial u_j}{\partial x_i} \right) \quad (14)$$

$$S_{ij} = \eta \left(\frac{\partial u_i}{\partial x_j} + \frac{\partial u_j}{\partial x_i} \right) = k \dot{\gamma}^{n-1} \left(\frac{\partial u_i}{\partial x_j} + \frac{\partial u_j}{\partial x_i} \right) \quad (15)$$

The rheological properties of the vinasse, the water and diluted dairy cow manure are shown in **Table 1**. It can be seen that the properties of the vinasse are closed to the properties of water. The difference between these two substrates is mainly the presence of suspensions. In anaerobic digestion process, the particles settle, accumulate at the bottom of the digester and result in the formation of sludge. In the present study, as a monophasic model is considered, the suspensions are not taken in account.

2.5 Flow field analysis

The Reynolds number for mechanical agitation of Newtonian fluids is [13, 18, 19]:

$$Re = \frac{\rho N d^2}{\mu} \quad (16)$$

where N is the impeller speed (rev.s⁻¹ or rps), ρ is the fluid density (kg.m⁻³), d is the impeller diameter (m) and μ is the dynamic viscosity (Pa.s).

The generalized Reynolds number valid for non-Newtonian fluids is [5]:

$$Re_g = \frac{\rho U_\infty^{2-n} d^n}{K \left(0.75 + \frac{0.25}{n} \right)^n 8^{n-1}} \quad (17)$$

where U_∞ is the average velocity of the fluid (m.s⁻¹), k is the consistency index (Pa.s ^{n}), n is the flow index and d is the reference length (m).

The evaluation of the energy consumption and consequently its economic impact is possible with the calculation of the power calculation. The power consumption P (W) calculation based on the torque of the impeller is:

$$P = 2\pi NT \quad (18)$$

where N is the impeller rotational speed and T is the impeller torque (N.m). The torque is defined as [20]:

$$T = \left(\int_S \left(\vec{r} * (\vec{\tau} \cdot \hat{n}) \right) dS \right) \cdot \hat{\alpha} \quad (19)$$

where S represents the surfaces including the rotating parts, $\vec{\tau}$ is the total stress tensor, \hat{n} is a unit vector normal to the surface, \vec{r} is the position vector and $\hat{\alpha}$ is a unit vector parallel to the rotation axis.

The mixing energy level (MEL) (W.m⁻³) is calculated by [21]:

$$MEL = \frac{P}{V} \quad (20)$$

where P is the power consumption (W) and V is the working volume (m³).

The flow rate through the moving zone Q (m³.s⁻¹) is used for the evaluation of the fluid circulation through the digester. We create a surface for the discharge zone

for computing the flow rate. The surface consists of two discs above and below the stirrer for the axial flow and a cylinder (AMI section) for the radial flow.

The power and flow (also called pumping number) numbers are two dimensionless numbers commonly used to characterize the stirred tank flows and mixing processes. The flow number is a measure of the pumping capacity of an impeller [13]. The power number is a dimensionless parameter that provides a measure of the power requirements for the operation of an impeller [13]. These two mixing parameters can be calculated from CFD results and allow to compare the results of simulations with the experimental results. In our case, the experimental values for hydrofoil impeller are N_P equal to 0.3 and N_Q equal to 0.56 [11, 22]. The power and flow numbers are respectively expressed by:

$$N_P = \frac{P}{\rho N^3 d^5} \quad (21)$$

$$N_Q = \frac{Q}{Nd^3} \quad (22)$$

The spatially average characteristic velocity gradient G (s^{-1}) is used for describing the rotational speed through the digester [23], as well as characterizing the turbulent shear rate [22]. It is defined with the following expression [22, 23]:

$$G = \left(\frac{\bar{\varepsilon}}{\nu} \right)^{1/2} \quad (23)$$

where ν is the kinematic viscosity and $\bar{\varepsilon}$ ($m^2 \cdot s^{-3}$) is the global average turbulent energy dissipation rate calculated as follow [22, 23]:

$$\bar{\varepsilon} = \left(\frac{N_P N^3 d^5}{V} \right) \quad (24)$$

The circulation time t_c is expressed by [22, 24]:

$$t_c = \frac{V}{N_Q N d^3} = \frac{V}{Q} \quad (25)$$

The vorticity ξ (s^{-1}) is a measure of the local rotation in the fluid. More specifically, it is a vector field that gives a microscopic measure of the rotation at any point in the fluid. The vorticity describes the local spinning motion. The helicity H provides indications on the alignment of the vorticity vector and the velocity vector U . It allows to illustrate the longitudinal vortices, or spiral motion, as is often found in vortex cores.

The vorticity is defined as the curl of the velocity vector:

$$\xi = \nabla \times U \quad (26)$$

The helicity is expressed as:

$$H = U \cdot \xi = U \cdot (\nabla \times U) \quad (27)$$

The angle between the vorticity vector and the velocity vector (which is 0° or 180° in a vortex core) is given by:

$$\alpha = \cos^{-1} \left(\frac{H}{|\xi||U|} \right) \quad (28)$$

2.6 CFD simulations

The numerical simulations are performed on OpenFOAM software. The PIMPLE algorithm is used, which is a combination of the PISO (pressure-implicit with splitting of operators) [25, 26] and SIMPLE (semi-implicit method for the pressure linked equations) [27] algorithms. The PISO algorithm is pressure implicit with splitting of operators [25] and allows the use of the sliding mesh method. The SIMPLE algorithm is the semi-implicit method for pressure linked equations [28]. The pimpleFoam solver assumes incompressible, unsteady and viscous flows. The simulations are launched in parallel on 16 processors. The simulation time, for which we get a steady state, is a few seconds. The calculation time is about a few days.

3. Results and discussions

3.1 Mesh

The tank geometry and the mesh are done on OpenFOAM and the impeller geometry on Sketch Up. Then, the OpenFOAM snappyHexMesh command is used to obtain the final mesh. The mesh is refined to meet the quality criteria of mesh such as cell skewness and mesh non-orthogonality. To meet these criteria, we reach a very large number of cells and thus long computing times. Consequently, we do not perform grid independence tests.

The surface mesh of the digester tank and the cross section of the mesh at the impeller level are shown in **Figures 3** and **4**.

The characteristics of the mesh are shown in **Table 2**. In total, this mesh is composed of 2,841,535 cells with mostly hexahedra. The total mesh faces is 9,150,640. The impeller edge has the larger amount of faces with a value of 465,732 due to its geometry. Concerning the interface between the moving zone and the stationary zone (AMI1 and AMI2), the two surface meshes must be identical with the same faces number in order to avoid numerical errors. Globally, the maximum cell skewness is 3.4 and the maximum mesh non-orthogonality is 65.0, which reflect an acceptable mesh quality. The dimensionless local Reynolds number y^+ is below 1.

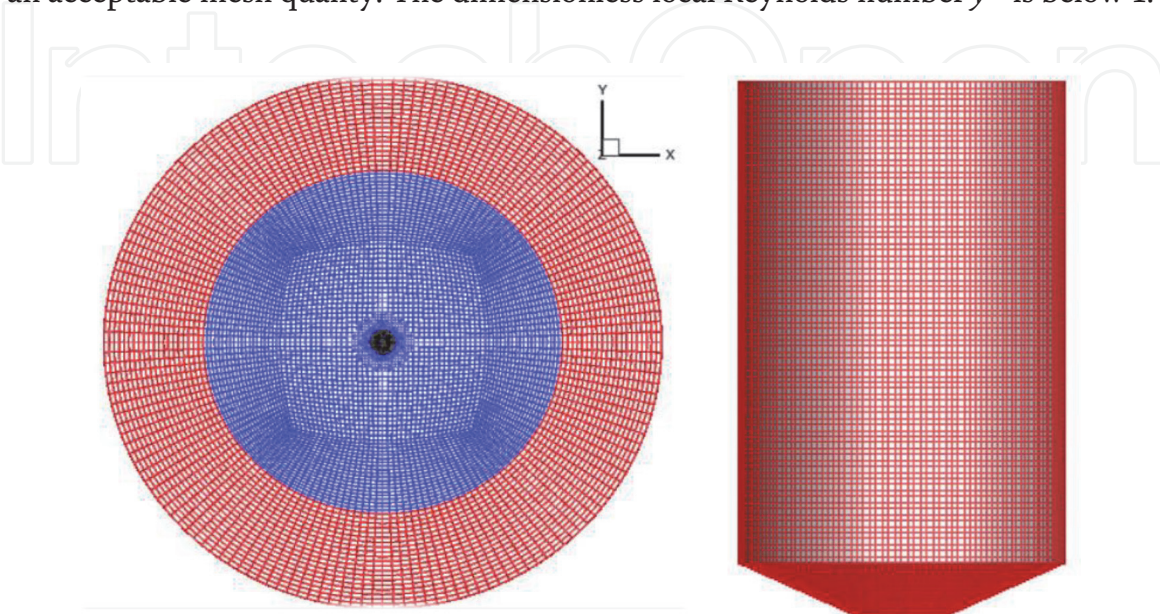


Figure 3.
Surface mesh of the digester: top (left) and wall (right).

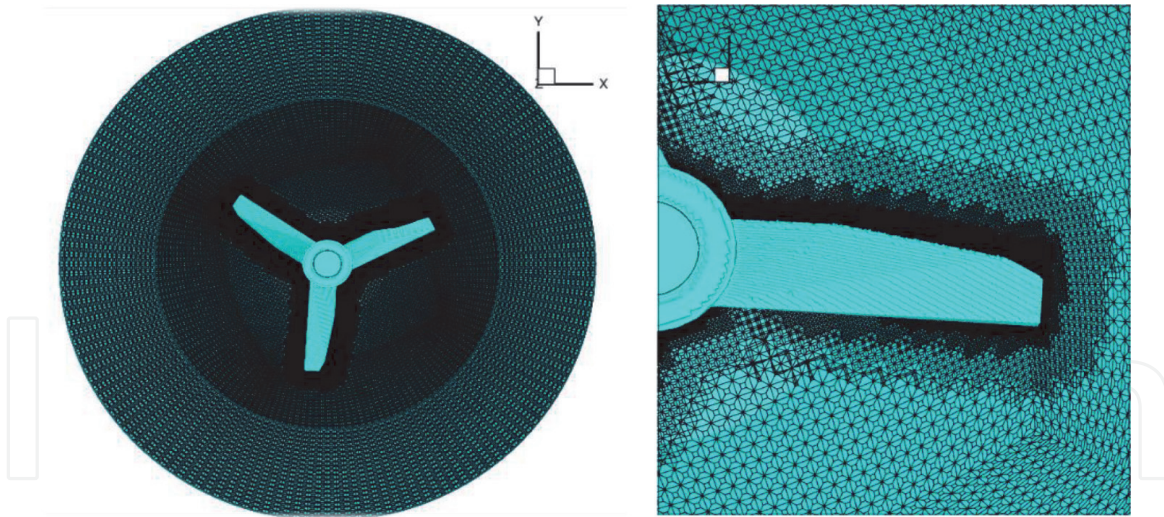


Figure 4.
Cross section of the mesh at the impeller level.

Characteristics		
Total mesh cells	2,841,535	
Total mesh points	3,485,073	
Total mesh faces	9,150,640	
Total mesh internal faces	8,591,189	
Number of hexahedra	2,578,249	
Number of prisms	10,298	
Number of wedges	3	
Number of polyhedra	252,985	
Maximum cell skewness	3.40025	
Maximum mesh non-orthogonality	65.0182	
Average mesh non-orthogonality	21.3783	
Breakdown of polyhedra by number of faces		
Faces	Number of cells	
<10	216,780	
≥10	36,205	
Patch topology		
Patch	Faces	Points
Upper edge (moving zone)	5719	5952
Bottom edge (moving zone)	4800	4881
Impeller edge (moving zone)	465,732	483,277
Upper edge (stationary zone)	3200	3360
Bottom edge (stationary zone)	3200	3360
Lateral wall (stationary zone)	25,760	25,760
AMI1	25,760	25,760
AMI2	25,760	25,760

Table 2.
Mesh characteristics.

3.2 Velocity profiles and shear stress

In this part, we present the simulation results for four rotational speeds: 20, 40, 60 and 100 rpm. **Figure 5** shows the cross section of the velocity field within the digester at the agitator height and **Figure 6** extends the longitudinal section of the velocity field.

The results obtained are consistent. In fact, by increasing the rotation velocity of the stirrer, the maximum velocity increases, the volume of dead zones decreases and the volume of continuously agitated zones increases. The maximum velocity value obtained for each case is the agitator velocity. The maximum velocity is obtained at the blade extremities. The velocity decreases gradually with the distance from the agitator.

For each case, we find that the velocity at the edges of the digester is zero. Likewise, the velocity at the axis of the agitator increases with the increase of the rotational speed. The interest of the study of the velocity field at this level relates in particular to the influence of the agitation on the biofilm which tends to develop on

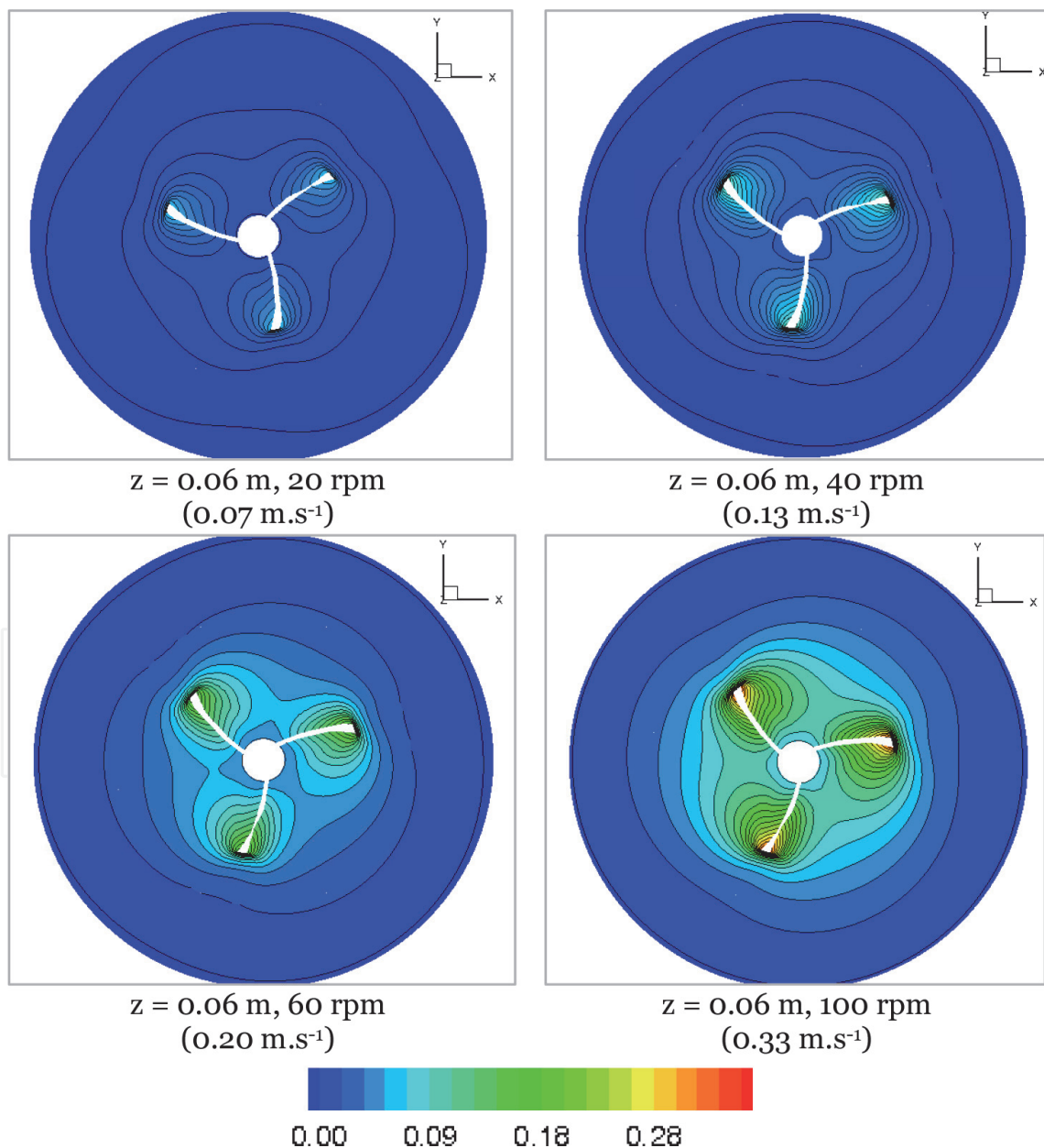


Figure 5. Axial cross-section of the velocity field ($m.s^{-1}$) within the digester at the agitator level ($z = 0.06 m$) for four rotational speeds: 20, 40, 60 and 100 rpm (the maximum velocity in $m.s^{-1}$ at the impeller extremity is mentioned below the figures).

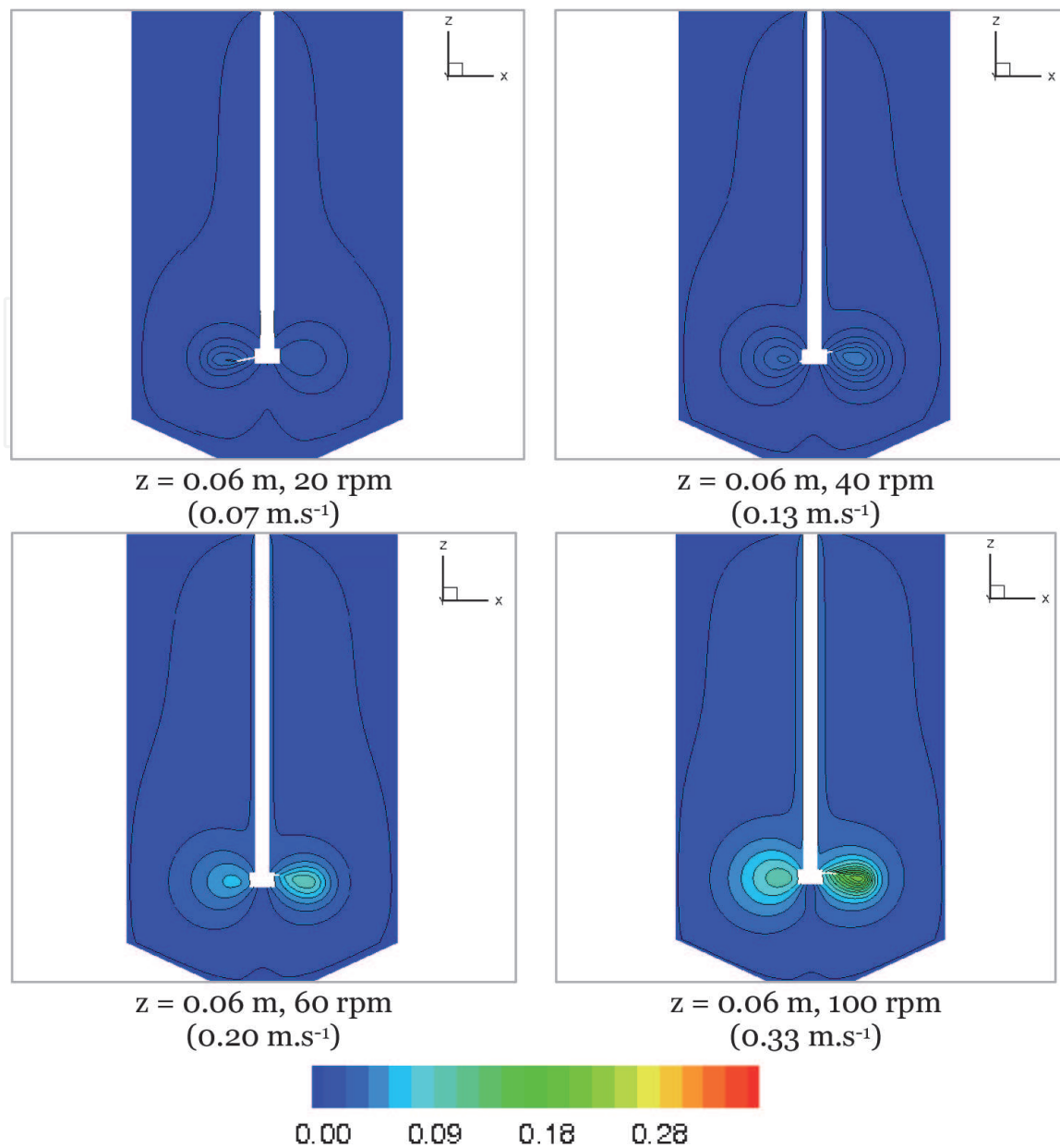


Figure 6.

Longitudinal cross-section of the velocity field (m.s^{-1}) within the digester for four rotational speeds: 20, 40, 60 and 100 rpm (the maximum velocity in m.s^{-1} at the impeller extremity is mentioned below the figures).

the axis of the agitator. The interest is even greater in the case of intermittent mixing. This mode of agitation is particularly interesting because it leads to the reduction of energy consumption. Overall, the optimization of the mechanical agitation must allow to properly stir the medium, so as to improve the biogas yields, while reducing the rotational speed and frequency of agitation.

From both the axial and longitudinal sections of the flow field, we observe that the maximum velocity field is mainly concentrated in the area close to the agitator and quickly becomes zero away from the influence zone of the impeller blades.

We assume that the dead zones are defined by a velocity magnitude less than 0.001 m.s^{-1} as [5]. Considering this hypothesis, we find that, in our case study, almost the whole area is dead zones except in the zone of influence of the agitator, which is more important with the increase of the rotation speed. Regarding the contours of the longitudinal cross-section, it can be seen that low-speed velocities are observed near the impeller axis. Furthermore, the area at the upper edges of the digester as well as the lower area of the conical section remains dead zones despite a rotational speed of 100 rpm. CFD simulations are useful for defining the volume of

dead zones. Indeed, the dead zones within a digester lead to the heterogeneity of the medium. There will be areas where the substrate will not be digested or acidic areas. This can eventually lead to intoxication of the digester generating significant costs on an industrial scale.

Experimentally it would result in an accumulation of solid and undigested matters, and thus the formation of sludge. It is therefore necessary to adapt the agitation according to the digester technology (with or without sludge bed). In addition, in the case of anaerobic digestion of a recalcitrant waste, such as vinasse, it is important to apply sufficient agitation to re-suspend the undigested matter in order to improve yields.

Similarly, since the upper part of the digester is not agitated, the digestion medium would not be homogenized. Overall, this mode of agitation (mechanical, a three-bladed agitator) would result in a significant stratification of the reaction medium with the presence of dead zones.

In view of the obtained results, it would be recommended to use a stirring system with several rows of blades to agitate the lower and upper areas of the digester to avoid stratification of the digestion medium. In addition, it would be desirable that the diameter of the stirrer be close to that of the digester in order to limit the development of biofilm on the walls. In addition, these simulations provide information on the velocity field within the digester as a function of agitator rotational speed; however, we have no information on their impact on the biochemical reactions and the biogas production and quality.

A study has been carried out on the impact of shear stress and impeller design on the production of biogas in anaerobic digesters [29]. An impact of the shear stress on the biogas production was highlighted [29] and the abrasion of the anaerobic sludge granule due to the shear rate increase above 5 s^{-1} [29, 30]. Therefore, it was suggested to estimate the shear stress value for the impeller type and mixing rotation [29]. In the present study, the shear stress is negligible in the digester expected at the wall and impeller levels. We obtained 0.31 Pa at 20 rpm and 1.24 Pa at 100 rpm at the tank wall. At the impeller wall, we reported 453 Pa at 20 rpm and 1883 Pa at 100 rpm. Therefore, the shear stress was multiplied by 4.15 at the impeller wall and by 3.9 at the digester wall, with the increase of the stirring speed from 20 to 100 rpm.

CFD simulations accompanied by experimental studies allow to relate the stirring velocity, the volume of dead zones, the homogenization of the medium (physicochemical properties) and the biogas yields. Thus, a better understanding of the physical phenomena involved in the digesters is necessary for the optimization of anaerobic digestion on an industrial scale. An experimental study on the anaerobic digestion of vinasse on this same geometry (digester and agitation system) would provide knowledge on the yields obtained with the velocity fields obtained in modeling. This would make it possible to relate the yields obtained experimentally to the flows.

3.3 Pressure

During the anaerobic digestion process, the pressure applied on the medium has an impact. Indeed, there are processes involving free microorganisms that are in the form of flocs or biofilm [31]. There are two types of biofilms, those formed on a mineral or organic support (fixed or mobile) and granules (natural agglomeration of microorganisms from a few tens of microns to several millimeters in diameter). In fact, the flow study through the digester provides information on the pressure imposed on the digestion medium. The interest is to evaluate the impact of pressure on the flocs and biofilms.

Figures 7 and 8 show the kinematic pressure in continuous flow regime at 40 and 100 rpm respectively. The pressure is due to the impeller rotation. At 20 rpm, it varies from 0 to $5.86 \cdot 10^{-5} \text{ m}^2 \cdot \text{s}^{-2}$ (0 to $5.86 \cdot 10^{-2} \text{ Pa}$). The pressure range at 40 rpm is -0.50 to $0.40 \text{ m}^2 \cdot \text{s}^{-2}$ which corresponds to -500 to 400 Pa . At 60 rpm, the pressure varies from -0.73 to $0.61 \text{ m}^2 \cdot \text{s}^{-2}$ (-730 to 610 Pa). At 100 rpm, it varies from -1.16 to $1.05 \text{ m}^2 \cdot \text{s}^{-2}$ (-1160 to 1050 Pa).

3.4 Turbulence phenomena analysis

The turbulence phenomena can be studied from different parameters. In the present study, we propose the description of the Reynolds number, the isotropic turbulence, the Q field, the Lambda2 fields and the vorticity.

Considering the impeller diameter for the characteristic length, the Reynolds number is 1326 at 20 rpm, 2651 at 40 rpm, 3977 at 60 rpm and 6629 at 100 rpm.

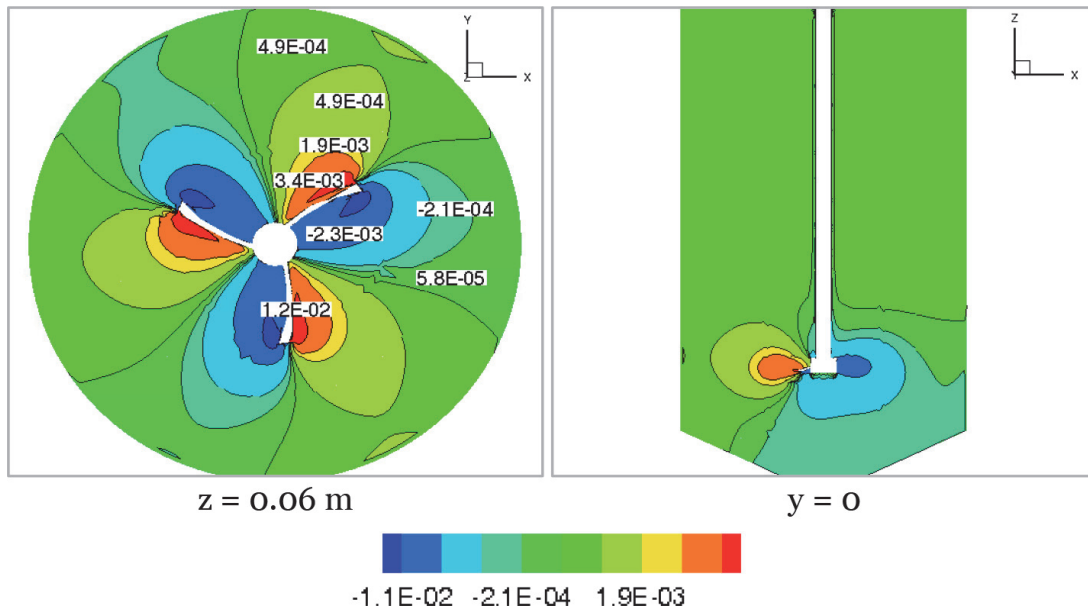


Figure 7. Kinematic pressure ($\text{m}^2 \cdot \text{s}^{-2}$) at 40 rpm ($z = 0.06 \text{ m}$, $y = 0$).

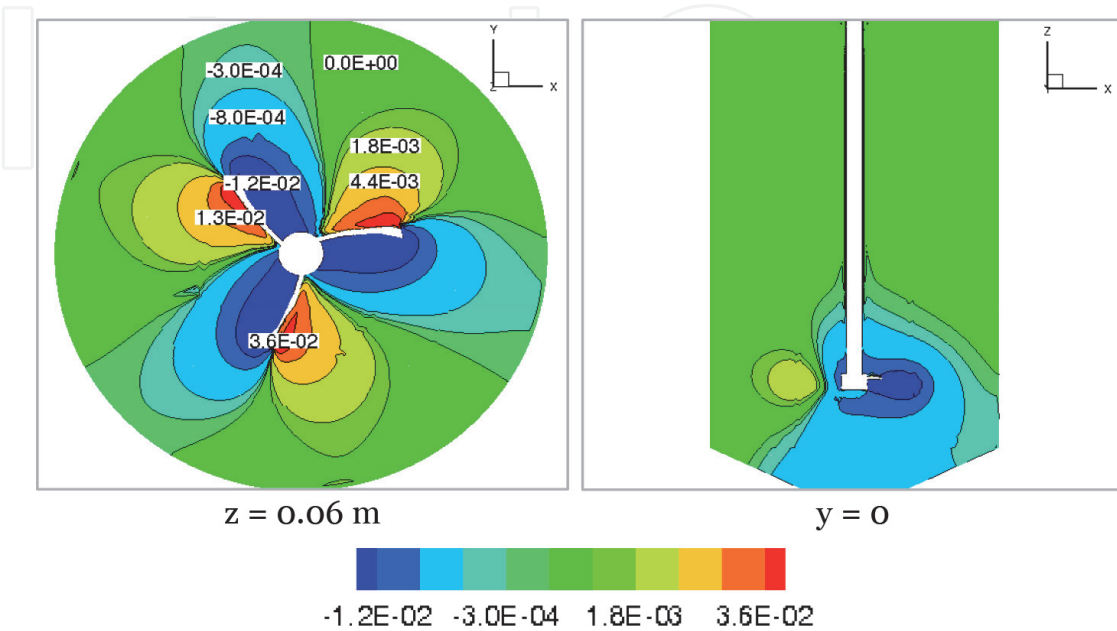


Figure 8. Kinematic pressure ($\text{m}^2 \cdot \text{s}^{-2}$) at 100 rpm ($z = 0.06 \text{ m}$, $y = 0$).

Therefore, local turbulence phenomena can occur around the impeller, however, the turbulence phenomena dissipate rapidly away from the impeller. If the isotropic turbulence k is very low, we consider that we are in a laminar regime. The maximum k value is $2.2 \times 10^{-16} \text{ m}^2 \cdot \text{s}^{-2}$ at 20 and 40 rpm, $3.0 \times 10^{-11} \text{ m}^2 \cdot \text{s}^{-2}$ at 60 rpm and $3.9 \times 10^{-8} \text{ m}^2 \cdot \text{s}^{-2}$ at 100 rpm. Therefore, we observe these local important values at the impeller level.

Q and Lambda2 fields provide a precise description of the turbulence and local rotation. The Lambda2 (s^{-2}) function object computes the second largest eigenvalue of the sum of the square of the symmetrical and anti-symmetrical parts of the velocity gradient tensor. Q iso-surfaces are good indicators of turbulent flow structures. The Q function object computes the second invariant of the velocity gradient tensor (s^{-2}):

$$Q = \frac{1}{2} \left[(\text{tr}(\nabla u))^2 - \text{tr}(\nabla u \cdot \nabla u) \right] \quad (29)$$

Figure 9 presents the velocity flood with the Lambda2 contours. The Lambda2 and velocity profiles are similar in zones between the blades but different at the impeller extremities.

Figure 10 shows the Q field at the impeller level at 40 and 100 rpm. The extremum values of the Q field are obtained at the impeller extremities. The Q field varies from -5171 to $39,405 \text{ s}^{-2}$ at 40 rpm and from $-27,000$ to $289,000 \text{ s}^{-2}$ at 100 rpm. The value is close to zero in areas away from the impeller. The Q field varies from -1383 to 8924 s^{-2} at 20 rpm and from -9314 to $94,137 \text{ s}^{-2}$ at 60 rpm.

The Lambda2 field at the impeller level at 40 rpm is shown in **Figure 11**. It varies from -3677 to $31,177 \text{ s}^{-2}$ at 40 rpm and from $-15,561$ to $226,008 \text{ s}^{-2}$ at 100 rpm. Both the Q and Lambda2 field maximum values are about seven times higher at 100 rpm than at 40 rpm. The Lambda2 field varies from -1125 to 8449 s^{-2} at 20 rpm and from -5234 to $73,482 \text{ s}^{-2}$ at 60 rpm.

Figure 12 presents the vorticity module (s^{-1}) at different digester heights in continuous flow regime at 40 rpm ($z = 0.06 \text{ m}$, $z = 0.08 \text{ m}$, $z = 0.259 \text{ m}$ and $y = 0$). The vorticity is a pseudo vector field that describes the local spinning motion (the curl of the velocity). The maximum vorticity module is 314.8 s^{-1} at 20 rpm, 621.7 s^{-1} at 40 rpm, 959.4 s^{-1} at 60 rpm and 1680.7 s^{-1} at 100 rpm.

The extremum values are observed at the impeller level. We notice that the maximum value of vorticity is multiplied by 2.7 from 40 to 100 rpm. We can

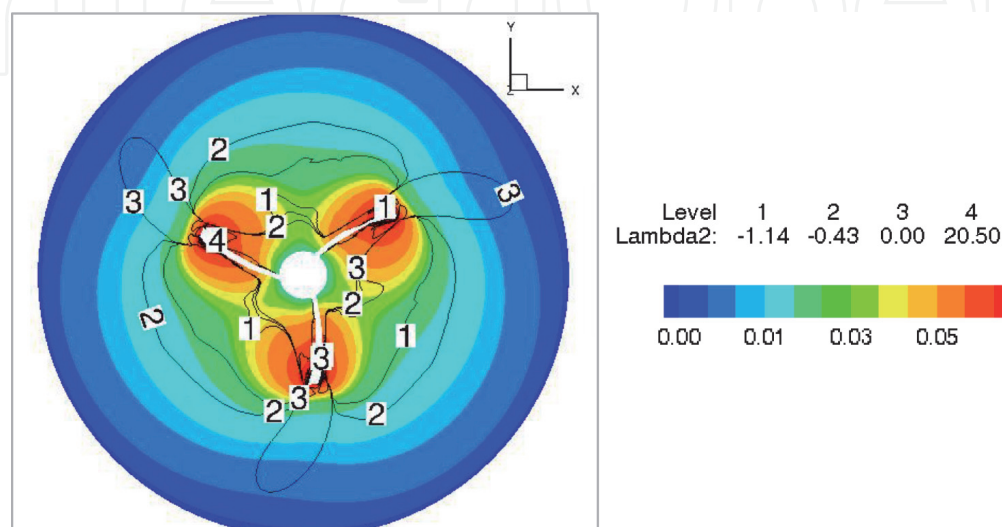


Figure 9.
 Velocity ($\text{m} \cdot \text{s}^{-1}$) flood and Lambda2 (s^{-2}) contour at 40 rpm ($z = 0.06 \text{ m}$).

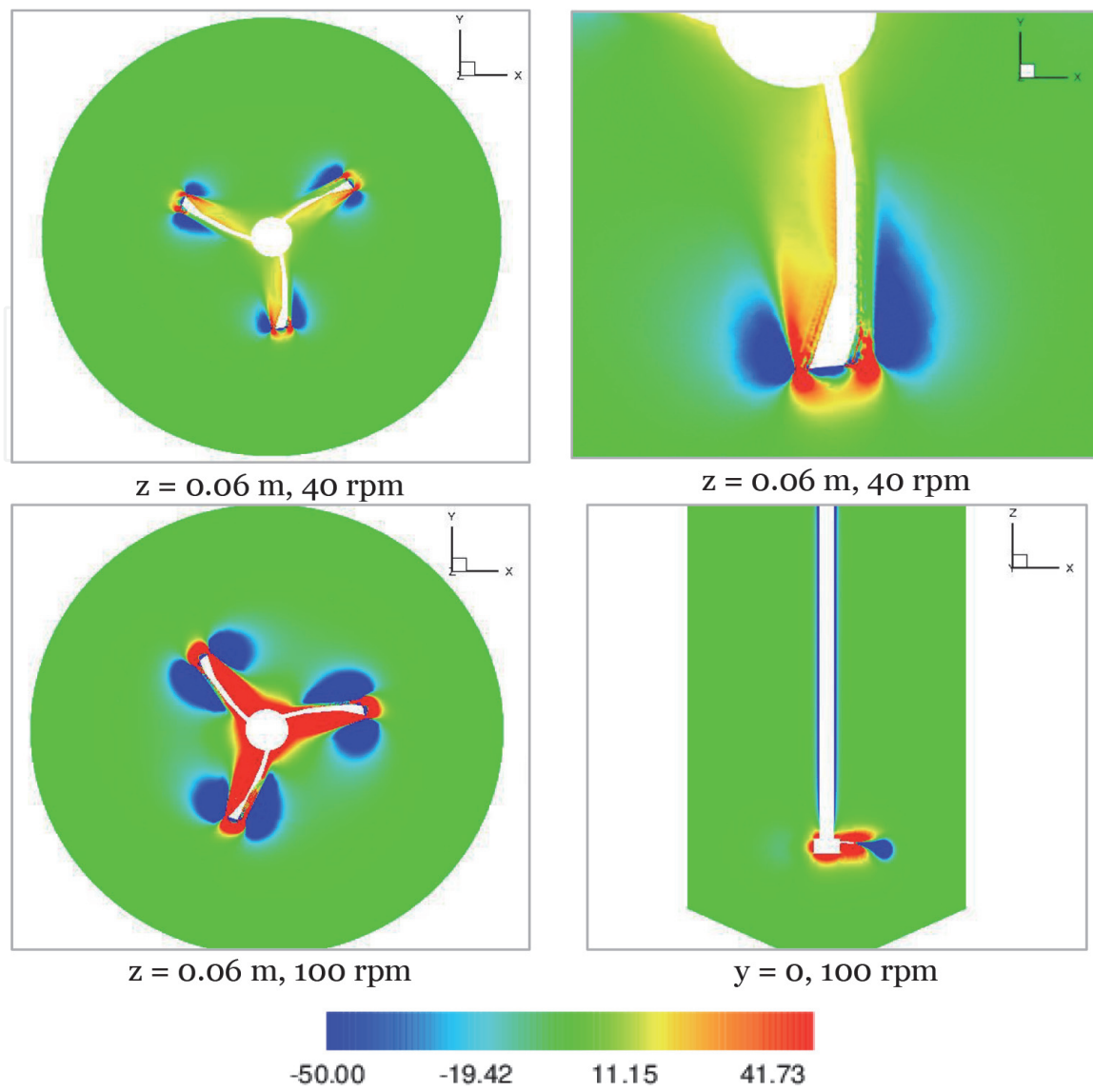


Figure 10.
 Q field (s^{-2}) at the impeller level at 40 and 100 rpm.

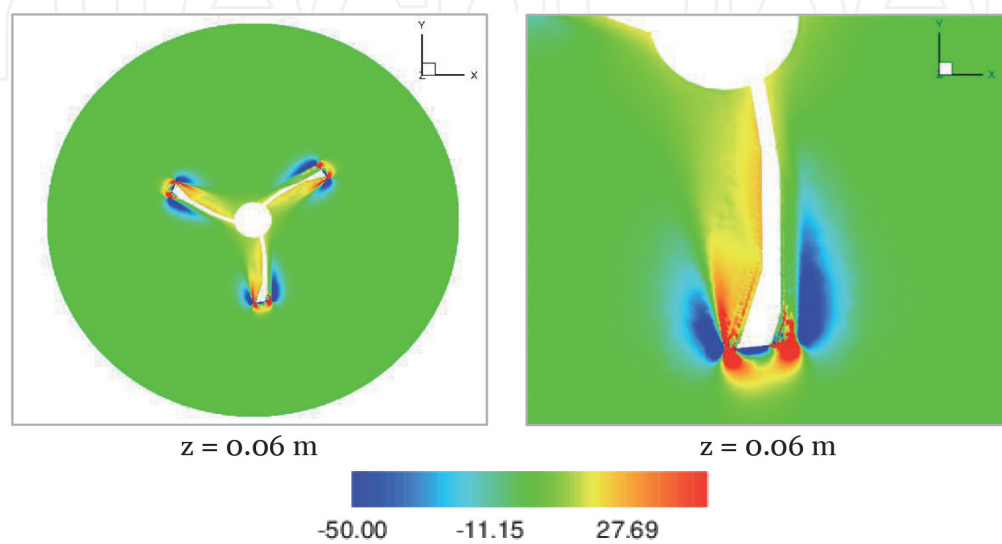


Figure 11.
 Λ_2 field (s^{-2}) at the impeller level at 40 rpm.

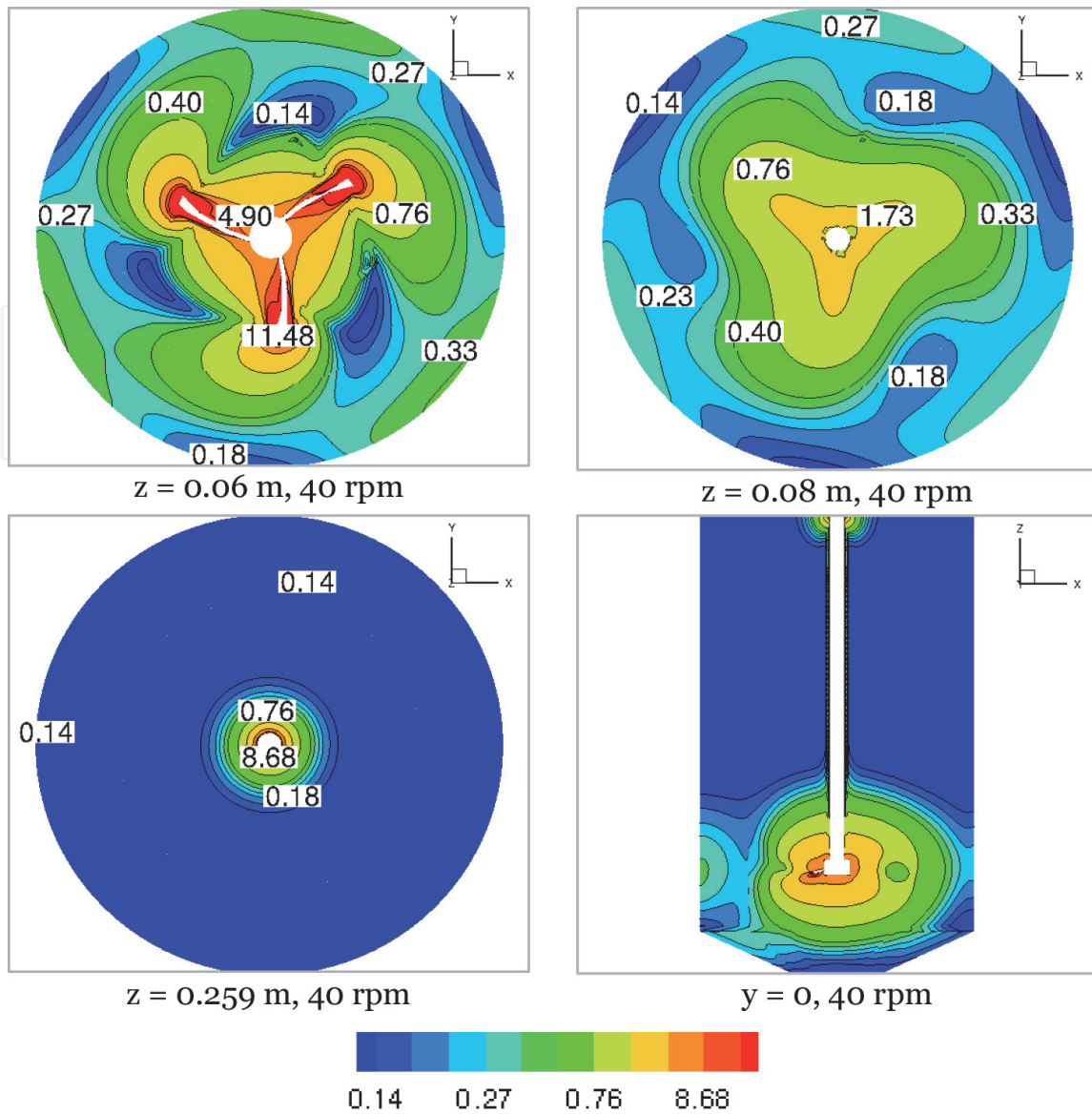


Figure 12. Vorticity module (s^{-1}) in continuous flow regime at 40 rpm ($z = 0.06$ m, $z = 0.08$ m, $z = 0.259$ m and $y = 0$).

consequently note that the variations of the Q and Lambda2 fields are more significant than the variation of the vorticity with the increase of the impeller mixing speed.

Figure 13 summarizes the variation of maximum vorticity, pressure, Q and Lambda2 values in function of mixing speed. The Q maximum value variation is the most pronounced among the parameters observed.

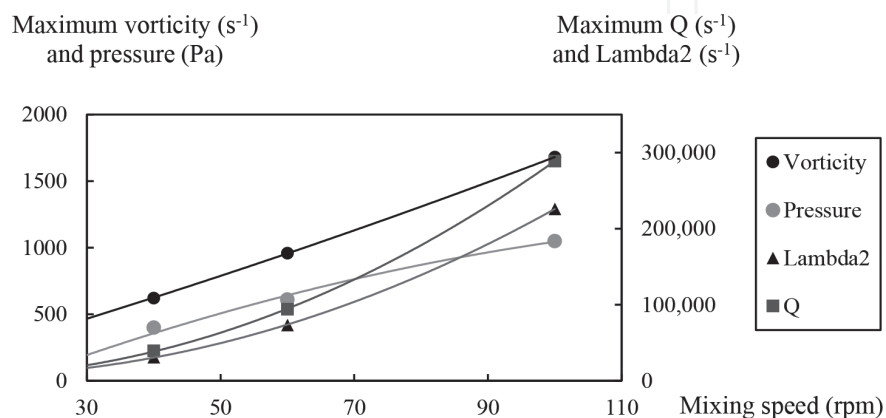


Figure 13. Variation of maximum vorticity, pressure, Q and Lambda2 values in function of mixing speed.

4. Conclusion

Three-dimensional CFD simulations of the mechanically stirred digester were carried out. The model was based on RANS equations and standard k-epsilon turbulence model and the fluid was Newtonian. The sliding mesh method was conducted to characterize the impeller rotation. The outcomes were the velocity profiles, the shear stress, the pressure and the turbulence phenomena analysis with the Q and Lambda2 fields, the Reynolds number, the isotropic intensity and the vorticity. The area of influence of the agitator was in the zone of the blades. The volume of dead zones was important for the four rotational velocities studied. The maximum velocity was observed at the blades extremities. In conclusion, several rows of paddles would be required to reduce the dead zone volume.

In perspective of this work, the flow study will be carried out for different tank geometry, agitation configuration and fluid rheology (non-Newtonian).

Acknowledgements

This work was supported by the Region Reunion (France) as part of the funding of a research thesis in the PIMENT laboratory at the Reunion Island University.


IntechOpen

Author details

Hélène Caillet*, Alain Bastide and Laetitia Adelard
PIMENT Laboratory, Reunion Island University, Saint-Denis, France

*Address all correspondence to: helene.caillet@univ-reunion.fr

IntechOpen

© 2020 The Author(s). Licensee IntechOpen. This chapter is distributed under the terms of the Creative Commons Attribution License (<http://creativecommons.org/licenses/by/3.0>), which permits unrestricted use, distribution, and reproduction in any medium, provided the original work is properly cited. 

References

- [1] Bollon J. Etude des mécanismes physiques et de leur influence sur la cinétique de méthanisation en voie sèche: essais expérimentaux et modélisation. Lyon, INSA, 2012.
- [2] Kerroum D, Mossaab B-L, Hassen MA. Production of biogas from sludge waste and organic fraction of municipal solid waste. INTECH Open Access Publisher; 2012.
- [3] López-Jiménez PA, Escudero-González J, Montoya Martínez T, Fajardo Montaña V, Gualtieri C. Application of CFD methods to an anaerobic digester: The case of Ontinyent WWTP, Valencia, Spain. *Journal of Water Process Engineering* 2015;7:131–40. <https://doi.org/10.1016/j.jwpe.2015.05.006>.
- [4] Vesvikar MS, Al-Dahhan M. Flow pattern visualization in a mimic anaerobic digester using CFD. *Biotechnology and Bioengineering* 2005;89:719–32. <https://doi.org/10.1002/bit.20388>.
- [5] Wu B, Chen S. CFD simulation of non-Newtonian fluid flow in anaerobic digesters. *Biotechnology and Bioengineering* 2007;99:700–11. <https://doi.org/10.1002/bit.21613>.
- [6] Koerich DM, Rosa LM. Optimization of bioreactor operating conditions using computational fluid dynamics techniques. *The Canadian Journal of Chemical Engineering* 2017;95:199–204. <https://doi.org/10.1002/cjce.22635>.
- [7] Fan W, Yuan L, Qu X. CFD simulation of hydrodynamic behaviors and aerobic sludge granulation in a stirred tank with lower ratio of height to diameter. *Biochemical Engineering Journal* 2018;137:78–94. <https://doi.org/10.1016/j.bej.2018.05.012>.
- [8] Foukrach M, Bouzit M, Ameer H, Kamla Y. Influence of the vessel shape on the performance of a mechanically agitated system. *Chemical Papers* 2019;73:469–80. <https://doi.org/10.1007/s11696-018-0606-4>.
- [9] Hoffmann RA, Garcia ML, Vesvikar M, Karim K, Al-Dahhan MH, Angenent LT. Effect of shear on performance and microbial ecology of continuously stirred anaerobic digesters treating animal manure. *Biotechnology and Bioengineering* 2008;100:38–48. <https://doi.org/10.1002/bit.21730>.
- [10] Caillet H, Adelard L. Start-Up Strategy and Process Performance of Semi-Continuous Anaerobic Digestion of Raw Sugarcane Vinasse. *Waste Biomass Valor* 2020. <https://doi.org/10.1007/s12649-020-00964-z>.
- [11] Wu B. Large eddy simulation of mechanical mixing in anaerobic digesters. *Biotechnology and Bioengineering* 2012;109:804–12. <https://doi.org/10.1002/bit.24345>.
- [12] Bugay S, Escudié R, Liné A. Experimental analysis of hydrodynamics in axially agitated tank. *AIChE Journal* 2002;48:463–475.
- [13] Paul EL, Atiemo-Obeng VA, Kresta SM, American Institute of Chemical Engineers, editors. *Handbook of industrial mixing: science and practice*. Hoboken, NJ: Wiley-Interscience; 2004.
- [14] Cortada-Garcia M, Dore V, Mazzei L, Angeli P. Experimental and CFD studies of power consumption in the agitation of highly viscous shear thinning fluids. *Chemical Engineering Research and Design* 2017;119:171–82. <https://doi.org/10.1016/j.cherd.2017.01.018>.
- [15] Launder BE, Spalding DB. *The numerical computation of turbulent flows* 1973:21.

- [16] Platteeuw PDA, Loeven GJA, Bijl H. Uncertainty Quantification Applied to the k-epsilon Model of Turbulence Using the Probabilistic Collocation Method. 49th AIAA/ASME/ASCE/AHS/ASC Structures, Structural Dynamics, and Materials Conference & 16th AIAA/ASME/AHS Adaptive Structures Conference & 10th, Schaumburg, IL: American Institute of Aeronautics and Astronautics; 2008. <https://doi.org/10.2514/6.2008-2150>.
- [17] Kuzmin D, Mierka O, Turek S. On the implementation of the $k - \epsilon$ turbulence model in incompressible flow solvers based on a finite element discretization 2007:8.
- [18] Wu B. Computational Fluid Dynamics Study of Large-Scale Mixing Systems with Side-Entering Impellers. Engineering Applications of Computational Fluid Mechanics 2012;6: 123–33. <https://doi.org/10.1080/19942060.2012.11015408>.
- [19] Marshall EM, Bakker A. Computational Fluid Mixing. In: Paul EL, Atiemo-Obeng VA, Kresta SM, editors. Handbook of Industrial Mixing, Hoboken, NJ, USA: John Wiley & Sons, Inc.; 2003, p. 257–343. <https://doi.org/10.1002/0471451452.ch5>.
- [20] Wu B. CFD analysis of mechanical mixing in anaerobic digesters. Transactions of the ASABE 2009;52: 1371–1382.
- [21] Wu B. CFD simulation of mixing in egg-shaped anaerobic digesters. Water Research 2010;44:1507–19. <https://doi.org/10.1016/j.watres.2009.10.040>.
- [22] Spicer PT, Keller W, Pratsinis SE. The effect of impeller type on floc size and structure during shear-induced flocculation. Journal of Colloid and Interface Science 1996;184:112–122.
- [23] Clark MM, Flora JR. Floc restructuring in varied turbulent mixing. Journal of Colloid and Interface Science 1991;147:407–421.
- [24] Alliet-Gaubert M, Sardeing R, Xuereb C, Hobbes P, Letellier B, Swaels P. CFD analysis of industrial multi-staged stirred vessels. Chemical Engineering and Processing: Process Intensification 2006;45:415–427.
- [25] Issa RI. Solution of the implicitly discretised fluid flow equations by operator-splitting. Journal of Computational Physics 1986;62:40–65.
- [26] Issa RI, Gosman AD, Watkins AP. The computation of compressible and incompressible recirculating flows by a non-iterative implicit scheme. Journal of Computational Physics 1986;62:66–82. [https://doi.org/10.1016/0021-9991\(86\)90100-2](https://doi.org/10.1016/0021-9991(86)90100-2).
- [27] Patankar SV, Spalding DB. A calculation procedure for heat, mass and momentum transfer in three-dimensional parabolic flows. Numerical Prediction of Flow, Heat Transfer, Turbulence and Combustion, Elsevier; 1983, p. 54–73. <https://doi.org/10.1016/B978-0-08-030937-8.50013-1>.
- [28] Caretto LS, Gosman AD, Patankar SV, Spalding DB. Two calculation procedures for steady, three-dimensional flows with recirculation. Proceedings of the third international conference on numerical methods in fluid mechanics, Springer; 1973, p. 60–68.
- [29] Aline L, Stéphane D, Philippe M, Fabrice B, Stéphane P, Michel F, et al. Impact of shear stress and impeller design on the production of biogas in anaerobic digesters.pdf. Bioresource Technology 2017.
- [30] Jiang J, Wu J, Poncin S, Li HZ. Effect of hydrodynamic shear on biogas production and granule characteristics in a continuous stirred tank reactor. Process Biochemistry 2016;51:345–51. <https://doi.org/10.1016/j.procbio.2016.05.011>.

<https://doi.org/10.1016/j.procbio.2015.12.014>.

[31] Moletta R. Technologies du traitement des effluents par méthanisation 2002:20.

IntechOpen

IntechOpen